



ELSEVIER

Contents lists available at ScienceDirect

Talanta

journal homepage: www.elsevier.com/locate/talanta

A vapor response mechanism study of surface-modified single-walled carbon nanotubes coated chemiresistors and quartz crystal microbalance sensor arrays



Hung-Ling Lu^a, Chia-Jung Lu^{a,*}, Wei-Cheng Tian^b, Horn-Jiunn Sheen^c

^a Department of Chemistry, National Taiwan Normal University, Taipei, Taiwan

^b Department of Electrical Engineering, National Taiwan University, Taipei, Taiwan

^c Institute of Applied Mechanics, National Taiwan University, Taipei, Taiwan

ARTICLE INFO

Article history:

Received 25 April 2014

Received in revised form

8 August 2014

Accepted 9 August 2014

Available online 19 August 2014

Keywords:

Carbon nano-tubes

Gas sensor

Volatile organic compounds

Chemiresistor

Quartz crystal microbalance

ABSTRACT

This paper compares the selectivity and discusses the response mechanisms of various surface-modified, single-walled carbon nanotube (SWCNT)-coated sensor arrays for the detection of volatile organic compounds (VOCs). Two types of sensor platforms, chemiresistor and quartz crystal microbalance (QCM), were used to probe the resistance changes and absorption masses during vapor sensing. Four sensing materials were used in this comparison study: pristine, acidified, esterified, and surfactant (sodium dodecyl sulfate, SDS)-coated SWCNTs. SWCNT-coated QCMs reached the response equilibrium faster than the chemiresistors did, which revealed a delay diffusion behavior at the inter-tube junction. In addition, the calibration lines for QCMs were all linear, but the chemiresistors showed curvature calibration lines which indicated less effectiveness of swelling at high concentrations. While the sorption of vapor molecules caused an increase in the resistance for most SWCNTs due to the swelling, the acidified SWCNTs showed no responses to nonpolar vapors and a negative response to hydrogen bond acceptors. This discovery provided insight into the inter-tube interlocks and conductivity modulation of acidified SWCNTs via a hydrogen bond. The results in this study provide a stepping-stone for further understanding of the mechanisms behind the vapor selectivity of surface-modified SWCNT sensor arrays.

© 2014 Elsevier B.V. All rights reserved.

1. Introduction

Volatile organic compounds (VOCs) represent a special category of hazardous substances that pose adverse effects to both the environment and human health [1]. Due to the diversity in chemical structures, the analyses of VOCs are usually performed using field sampling methods (i.e., canisters or adsorbent tubes) followed by in-lab analysis using a gas chromatograph–mass spectrometer (GC–MS) [2]. Although these analytical methods provide accurate assessments of VOC concentrations, they are often too expensive for continuous use and/or real-time analyses. On the other hand, chemical sensor arrays with cross sensitivity to VOCs can provide sufficient selectivity and detection limits for applications where immediate attention or continuous monitoring is called for [3].

Over the past few decades, several types of chemical sensors have been developed for the purpose of volatile compound or scent detection [4]. These sensor applications include metal oxide sensors [4], acoustic wave sensors (i.e., QCM and SAW) [5,6], optical sensors [7–9], and chemiresistors [10–12]. Recent research effort has been focused on improving the performance of these sensors by either employing nano structures to conventional materials such as metal oxide [13], or by applying newly developed nano materials such as metal nanoparticles [8–12] and nano carbon materials [14–16].

Among these newly developed nano materials for chemical sensing applications, carbon nanotubes have drawn much attention due to their highly adsorptive surfaces and their susceptible conductivity to environmental changes. Both single-walled carbon nanotubes (SWCNTs) and multi-walled carbon nanotubes (MWCNTs) have been demonstrated as highly sensitive materials for gas and vapor detection [14,17]. The earliest gas sensor employing SWCNTs was a field effect transistor device that measured the conductivity changes of a single carbon nano-tube [18]. Several recent studies have shown that measuring the film of randomly stacked CNTs on an interdigit electrode can also achieve a highly sensitive chemiresistor

* Correspondence to: No. 88, Sec. 4, Ting-Chou Rd., Taipei City, ROC, 11677, Taiwan. Tel.: +886 2 77346132; fax: +886 2 29324249.

E-mail address: cjlu@ntnu.edu.tw (C.-J. Lu).

frequency shift and voltage signal was recorded via a data acquisition interface card (DAQ-Pad 6015, National Instruments, USA). The software for continuous acquisition of frequency and voltage changes was written in-house using LabVIEW.

2.4. Instruments and apparatus

The infrared spectra of SWCNTs during the synthetic process were measured by FTIR (Spectrum RX-1, Perkin Elmer). A field emission scanning electron microscope (FE-SEM, S4800, Hitachi, Japan) was used to observe the image of the SWCNT film. A frequency counter (HP-5313A, Agilent, USA) and a resistance meter (model 6487, Keithley, USA) were used to monitor the oscillating frequency of QCM and resistance changes of chemiresistor during the spray coating of SWCNTs.

2.5. Vapor testing system

Test vapor was generated by a dynamic dilution system consisting of three mass flow controllers, stainless steel or Teflon manifolds, adsorbent traps, and a solvent evaporator. Clean background air was generated by passing compressed air through the tandem traps of a molecular sieve, charcoal, and a highly efficient particle filter (HEPA) to remove moisture, VOCs, and fine particles, respectively. The temperature was maintained at 25 ± 1 °C and relative humidity was kept below the lowest readable level ($< 1\%$) for a humidity meter (DO9861T-R1, Delta Ohm, Padua, Italy). The organic vapor concentration was generated by passing the background air through a bubbler to produce a saturated vapor concentration, and was diluted with different ratios of background air, and both were controlled using mass flow controllers (5850i, Brooks Instrument, PA). Two solenoid 3-way valves were connected to the front of the test cell and vent that allowed computer-controlled switching between the background air and the test vapor concentration. The generated vapor concentration was confirmed by GC-FID (HP5890, Agilent). The test cell that was used to house both the sensor arrays had an internal volume of ~ 250 mL. The volumetric flow rates were maintained at 5 L/min to ensure that the switching between test atmosphere and background air could be achieved in a few seconds.

3. Results and discussion

3.1. Characterization of surface modified SWCNTs

Fig. 2 shows the FTIR spectrums of pristine SWCNT, SWCNT-COOH, SWCNT-ESTER, and SWCNT-SDS. The pristine SWCNTs showed two small absorbance bands located at 1570 cm^{-1} that represented C=C stretching. Another small absorbance at 3410 cm^{-1} indicated a small fraction of oxidization on the surface of “as-purchased” SWCNT. After the acidification to SWCNT-COOH, narrower and sharper bands appeared at $1580\text{--}1750\text{ cm}^{-1}$ which indicated the absorbance of the C=O and COO⁻ functional groups. Another huge and broad absorbance band at $3000\text{--}3600\text{ cm}^{-1}$ was the contribution of -OH on the carboxylic acid group. When the SWCNT-COOH was further converted to a SWCNT-ESTER, the broad absorbance band at $3000\text{--}3600\text{ cm}^{-1}$ disappeared. Instead, a group of sharp absorbance peaks was seen at $2800\text{--}3000\text{ cm}^{-1}$, which indicated the replacement of -OH by the long alkane chain (-CH₂-, sp³) of an ester group (i.e., from -COOH to -COOR). The FTIR spectrum of the SWCNT-SDS showed both the similar signature of sp³ band from the long alkane chain of SDS and the absorbance signals of pristine SWCNT. These FTIR spectrums confirmed the changes in chemical structure as we progressively modified the SWCNT.

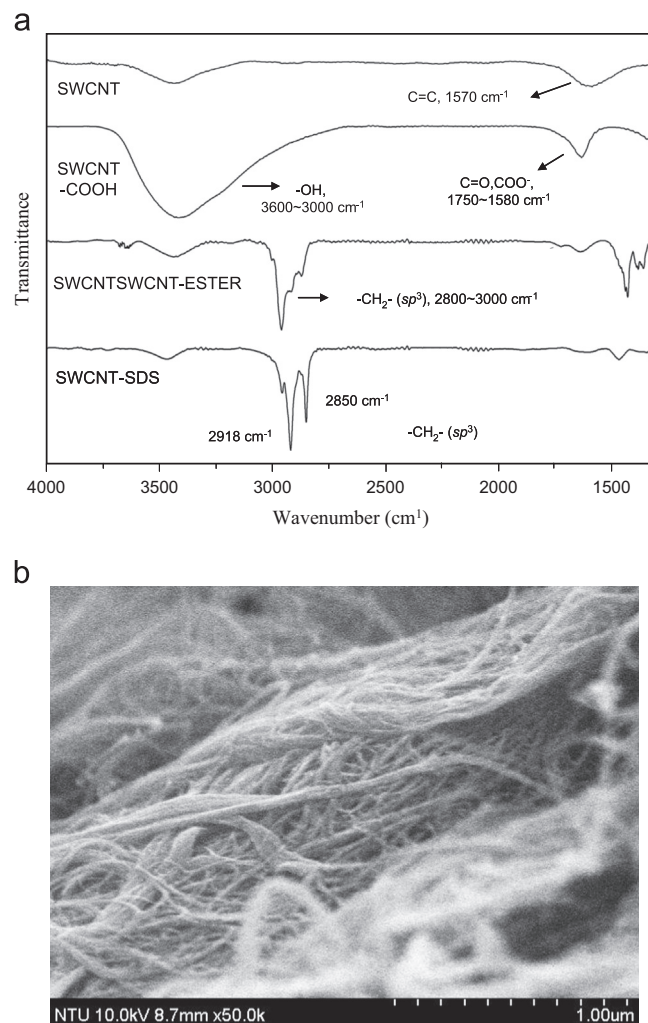


Fig. 2. (a) Infrared spectra of SWCNTs with and without surface modifications (b) SEM image of spray-coated SWCNT film.

Fig. 2b shows an example SEM image of a spray-coated SWCNT-ESTER film. The morphologies of all four SWCNT sensing films were very similar regardless of surface modification. The randomly stacked nanotubes created a naturally porous film. The pores among these randomly stacked nanotubes were ranged from submicron to several microns and were beneficial for rapid gas diffusion into the film. The gas response times of such a porous sensing film were expected to be short. A different study demonstrated by Feller et al. using polymer-coated CNTs as sensing film showed a faster rate of response equilibrium while significantly reducing the film thickness [33]. This showed how the diffusion through the polymer matrix contributed significantly to the response time. Unlike the film created by dense polymer coatings where gas diffusion time through sensing film contributes significantly to sensor response time, the small difference in the thickness of SWCNT film was expected to have a minor effect on the response time due to its porous structure.

3.2. Response time differences between QCMs and chemiresistors

Fig. 3 shows examples for the response signals of a chemiresistor (CR) and that of a QCM sensor. The chemiresistor circuitry was configured in such a way that the increases in resistance caused the increases in output voltage. The frequency shift of the QCM during vapor adsorption was always negative. The response signals of the QCM were reversed and overlapped with the chemiresistor signal in

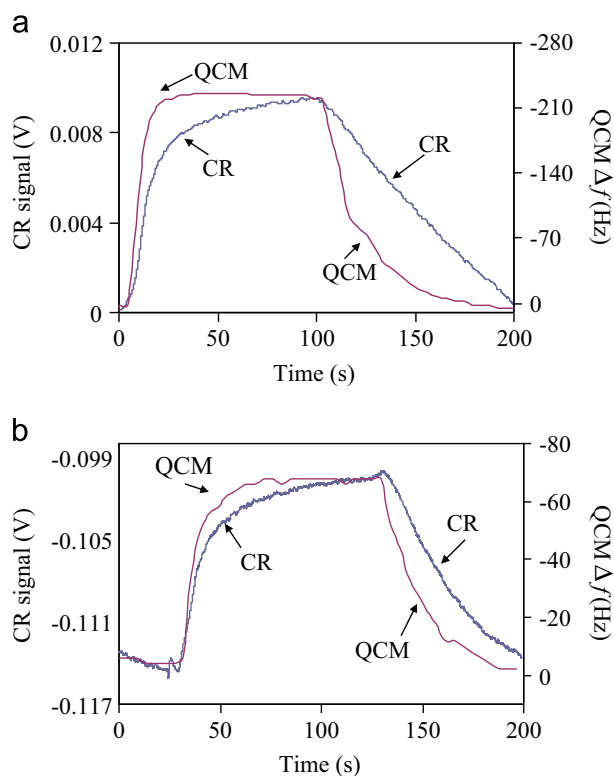


Fig. 3. Examples for overlapped response signals of QCM and chemiresistor (CR) (a) SWCNT-SDS sensors and the response to 3000 ppm butanol. (b) SWCNT-ESTER sensors and the response to 3500 ppm butyl acetate. (note: 2nd y-axis is in reversed order).

order to compare the times required for reaching equilibrium for both sensors. Fig. 3a shows the response signals of SWCNT-SDS-coated QCM and CR to 3000 ppm butanol. Fig. 3b shows the signals of SWCNT-ESTER-coated QCM and CR to 3500 ppm butyl acetate. In both cases, the responses of the QCM reached equilibrium faster than the chemiresistor did. Similar results were observed in all cases of pristine SWCNT, SWCNT-SDS and SWCNT-ESTER. This was particularly noteworthy because both sensors were coated with the same material at a similar thickness. As shown in the SEM image (Fig. 2b), the porous nature of randomly stacked SWCNT films was expected to enable a fast equilibrium between the gas phase and the surface adsorption. However, the increases in resistance require vapor molecules to intercalate between the junctions of two nanotubes. A proposed response mechanism is illustrated in Fig. 4. With the onset of vapor concentration, the vapor molecules diffused rapidly into the porous SWCNT films and were readily adsorbed onto the non-overlapped surfaces of SWCNTs. This was the adsorption-mass-increase stage, and a frequency shift of the QCM occurred. The remaining kinetic energy of adsorbed vapor molecules allowed the molecules to move into the overlapped regions between the nanotubes. The overlapped regions provided van der Waal attraction from both sides of the nanotube wall, which was better stabilized by the adsorbates. Thus, the adsorbed molecules had a greater tendency to stay within the overlapped regions. The swelling between carbon nanotubes needed to overcome the attractions between nanotube surfaces and a slight displacement of these nanotubes. Therefore, even though it was thermodynamically favorable for adsorbed molecules to partition into the overlapped regions between SWCNTs, a certain amount of reaction time was still required to complete the displacement of SWCNTs during the swelling. The response behavior of SWCNT-COOHs differed from that of the other three sensing materials, which will be addressed in the following sections.

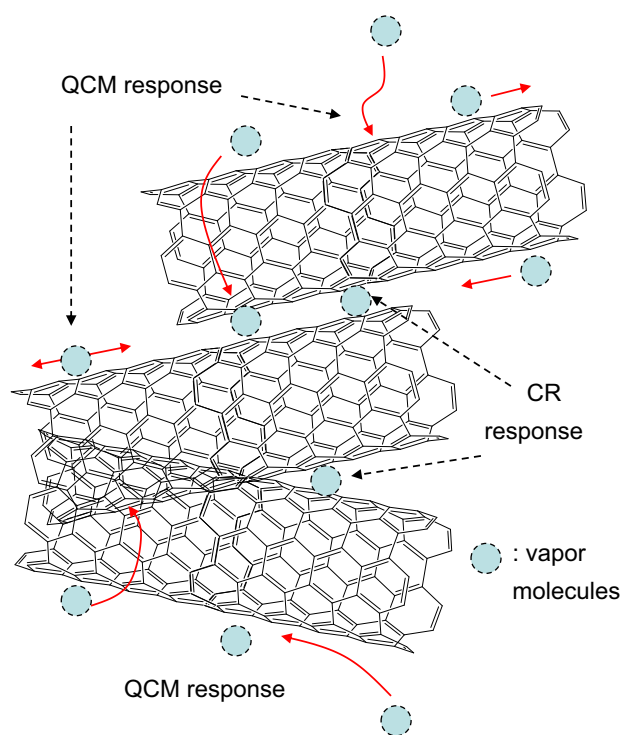


Fig. 4. Scheme for the response mechanism of pristine SWCNT-coated QCMs and chemiresistors.

3.3. Response signals of surface modified SWCNTs

Fig. 5 shows examples of the response signals for both a non-polar vapor (i.e., octane) and a highly polar vapor (i.e., butanol) for the four SWCNTs coated on both CR and QCM. As both Fig. 5a and b show, the coating of SDS on SWCNTs can significantly enhance the response for QCM sensors, which means an increase in vapor partition. When SDS was coated on the SWCNTs, the static charge of the $-\text{SO}_3^- \text{Na}^+$ terminal was attracted to the surface of the SWCNTs due to the highly polarizable conjugating electrons on the surface of the SWCNTs. After we had rinsed the SWCNT-SDS with toluene, the excessive SDS was eliminated leaving only the strongly adsorbed SDS that bind to the surface via a static charge-induced dipole attraction. The long alkane chain of the SDS layer provided an additional “stationary phase” for the partition of hydrophobic compounds. Hydrophilic compounds are more likely to be attracted by the $-\text{SO}_3^- \text{Na}^+$ group of SDS. When octane was absorbed by SWCNT-SDS, octane could partition into the overlapped alkane chain “spacer” and caused swelling between the nanotubes. As a result, the increased absorption of octane on SWCNT-SDS QCM showed an equivalent increase in the responses on the SWCNT-SDS chemiresistor. In the case of butanol, the SWCNT-SDS chemiresistor did not show sensitivity enhancement that matched the increase in absorption mass. This was because the overlapped regions of SWCNT-SDSs were spaced by non-polar alkane chains. Butanol was greatly attracted to the $-\text{SO}_3^- \text{Na}^+$ site near the SWCNT surface. An increase in mass adsorption can be seen in the QCM responses (Fig. 4b). The effectiveness of increasing the distances between SWCNT-SDS nanotubes by butanol adsorption was reduced because it did not contribute to the swelling of the non-polar end of the SDS shell. Also, the static charge of the $-\text{SO}_3^- \text{Na}^+$ site hindered the hydrogen bond formation of *n*-butanol directly to the surface of the SWCNTs. The possibility of reducing conductivity by scattering points [39,40] created from *n*-butanol adsorption was reduced; therefore, the resistance change exerted by *n*-butanol adsorption was less sensitive.

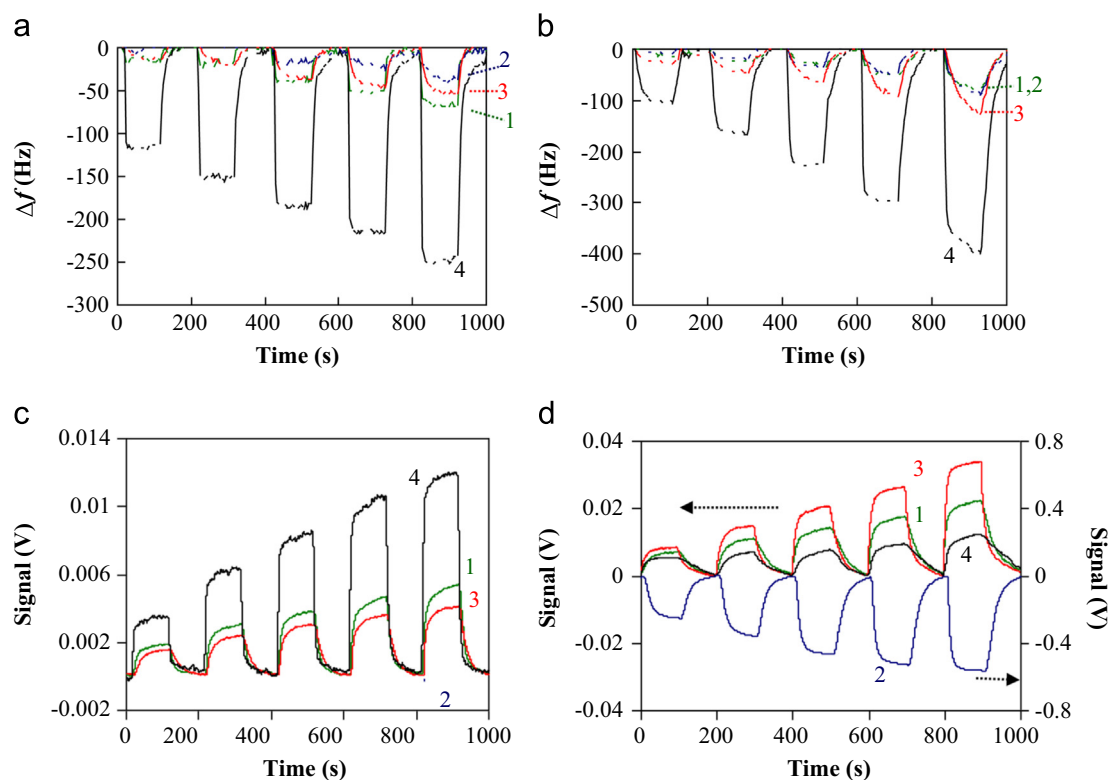


Fig. 5. Vapor responses of various SWCNT-coated QCMs and chemiresistors. Test concentrations: octane: 1916–9580 ppm; butanol: 981–4866 ppm. (a) QCM vs. octane (b) QCM vs. butanol (c) chemiresistor vs. octane (d) chemiresistor vs. butanol.

SWCNT-COOHs showed a sensing behavior that was more distinct than that of the other three materials. Judging from the response of the SWCNT-COOH-coated QCM, there was only a relatively small but detectable amount of octane adsorption on the SWCNT-COOH. However, the SWCNT-COOH-coated chemiresistor showed absolutely no response to octane even at very high concentrations. On the other hand, SWCNT-COOHs showed a higher adsorption mass for butanol than that of either pristine SWCNTs or SWCNT-ESTERS, but lower than that of SWCNT-SDSs. Surprisingly, a huge reverse response (i.e., resistance decrease) was seen with the SWCNT-COOH chemiresistor (Fig. 5d). It should be noted that the scale of the second y-axis on the right of Fig. 5d for SWCNT-COOH is 20 times larger than the scale of the first y-axis for the other three chemiresistors.

Unlike the NH_3 or NO_2 that were used as target gases for SWCNT sensors in earlier studies [25,41], nonpolar VOCs, such as octane, lack the ability to change the electron density of SWCNT. Therefore, the chemiresistor responses of octane on SWCNT, SWCNT-ESTER and SWCNT-SDS are mainly due to the swelling between the carbon nanotubes that increases the resistance of electron-hopping at the junctions of nanotubes. SWCNT-COOH has very strong hydrogen bonding terminals. The massive hydrogen bonds at the junction regions held SWCNT-COOH nanotubes tightly together. The adsorbed octane on the surface was not capable of breaking the hydrogen bond “interlocks” between the SWCNT-COOH nanotubes (Fig. 6). Therefore, SWCNT-COOH-coated chemiresistors showed no response to octane.

Butanol is neither a strong electron donor nor an acceptor by comparison with either NH_3 or NO_2 . The increases in resistance indicate that the swelling remains to be the dominant mechanism for pristine SWCNT, SWCNT-SDS and SWCNT-ESTER chemiresistors. However, a huge decrease in resistance was observed when butanol was adsorbed onto SWCNT-COOH. Although the hydroxyl group ($-\text{OH}$) of butanol can act as a hydrogen bond donor or acceptor, its acidity is much lower than that of the carboxyl group

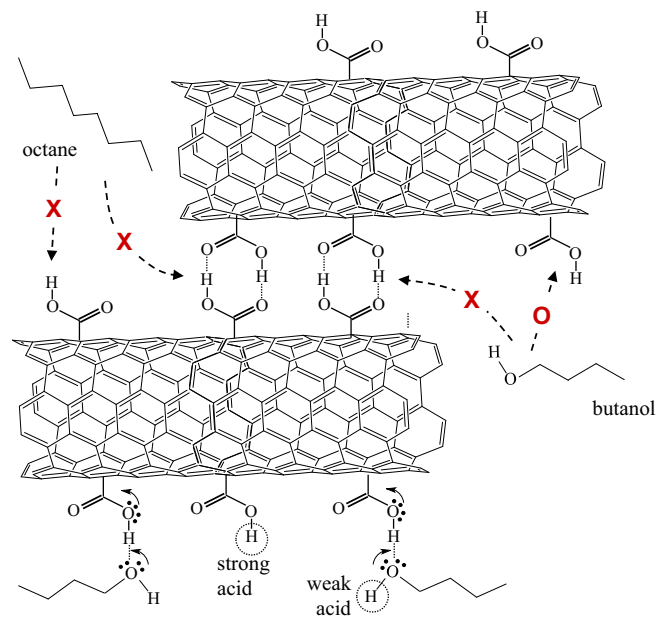


Fig. 6. Scheme for the response mechanisms of SWCNT-COOH-coated chemiresistors.

($-\text{COOH}$). Therefore, we believe that hydroxyl groups accept protons from carboxyl groups when hydrogen bonds are formed, which allows the conjugating electrons of carboxylic groups to increase the electron density on carbon nanotubes and the conductivity of SWCNT-COOH film to increase. This reverse response is also known as Negative Vapour Coefficient (NVC) and is sometimes observed with Poly aniline (PANI) or other Intrinsically Conducting Polymers (ICP) [42,43].

3.4. Calibration lines of SWCNTs coated QCMs and chemiresistors

Fig. 7 shows the calibration lines of toluene for both QCM and chemiresistor arrays. The y-axis units for the QCM arrays were $\Delta f_i / \Delta f_s$, which stands for the vapor response frequency shift (Δf_i) normalized to the frequency shift induced by the coating thickness (Δf_s) of SWCNT film. The output signal of the chemiresistor was voltage, which was converted to the change in resistance (ΔR) using Ohm's law. The y-axis units for the chemiresistor calibrations were expressed as $\Delta R/R_0$, which represented a change in the resistance normalized to the film resistance (R_0) in clean air. The units on the y-axis of Fig. 7a and b are changes in parts per million (ppm). The calibration lines of QCM for all SWCNTs (Fig. 7a) were linear over a wide range of vapor concentrations. On the contrary, the calibration lines of chemiresistors were all curved for pristine SWCNTs, SWCNT-ESTERS, and SWCNT-SDSs. There was no calibration data for toluene from the SWCNT-COOH-coated chemiresistor, because it did not respond to toluene. Due to the high signal-to-noise ratios of chemiresistors, the responses of this array can be measured at lower concentrations. The inset of Fig. 7b shows the calibration lines of a chemiresistor array at a lower concentration range. The chemiresistor responses appeared to be closer to linear at low concentrations and gradually leveled off at high concentrations.

The linear calibrations of the QCM sensors indicated that the partition coefficients for surface adsorption over the tested concentration range were constant. The surface adsorption mass was

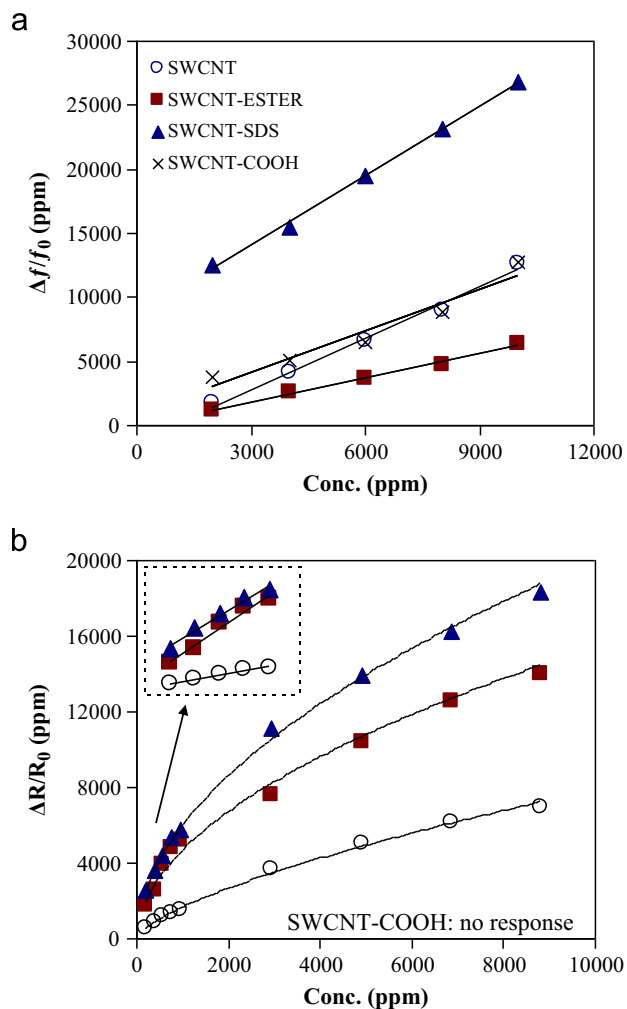


Fig. 7. Examples of toluene calibration curves for SWCNT-coated (a) QCMs and (b) chemiresistors. The inset in (b) shows the blow-up of low concentration responses for chemiresistors.

always in a linear proportion to the concentration in the test atmosphere. However, increases in adsorbed molecules at high concentrations did not seem to swell the nanotube films as effectively as they had at lower concentrations. As illustrated in Fig. 4, vapor molecules were first adsorbed onto the non-overlapped surface of SWCNTs. Some kinetic energy remained on the adsorbed molecules, which allowed them to move along the SWCNT surface, and some of them were stabilized at the junction point of the nanotubes. In general, the overlapped regions provided better stabilization by offering the conjugating π -electrons for dispersion attractions from both sides of two adjacent SWCNT walls. A partition equilibrium exists between the non-overlapped surface and the overlapped regions. The concentration inside the overlapped region could be higher than that on the non-overlapped surface due to stabilization. At low concentration, adsorbed molecules were rapidly diffused into the overlapped region and effectively increased the resistance at the junction point. When vapor concentrations were high, these small overlapped regions approached saturation. When a second or third layer of adsorption occurred inside the overlapped region, the stability from both SWCNT walls was reduced due to the increased separation between SWCNT walls. The partition into the overlapped region became less favorable than it was at low concentration. Therefore, the calibration lines of swelling-dependent SWCNT chemiresistors appeared to be nonlinear over a large concentration range. This adsorption/diffusion behavior was previously fitted to an LHC (i.e., Langmuir Henry Clustering) model. Details regarding the use of this model can be found elsewhere [33,44].

In addition to the discrepancy in the linearity between the QCM and chemiresistor calibrations, the relative sensitivities of these SWCNTs were also different on two platforms. The sensitivity trend for toluene on the QCM array was SWCNT-SDS > SWCNT = SWCNT-COOH > SWCNT-ESTER. The sensitivity order of toluene on the chemiresistor array was SWCNT-SDS > SWCNT-ESTER > SWCNT \gg SWCNT-COOH (i.e., no response). As indicated earlier, the responses of the QCM revealed the partition coefficients between the air and the SWCNT film. The responses of the chemiresistors were affected by at least three factors: the partition between the air and the SWCNT surfaces, the partition between non-overlapped and overlapped surfaces, and the effectiveness of the swelling. The effectiveness of the swelling is mainly determined two factors: the free volume associated with the adsorbed organic molecules, and the attractions between the nanotubes. Both factors could be affected by the surface modification of the SWCNTs. For example, the strong hydrogen bonds between the

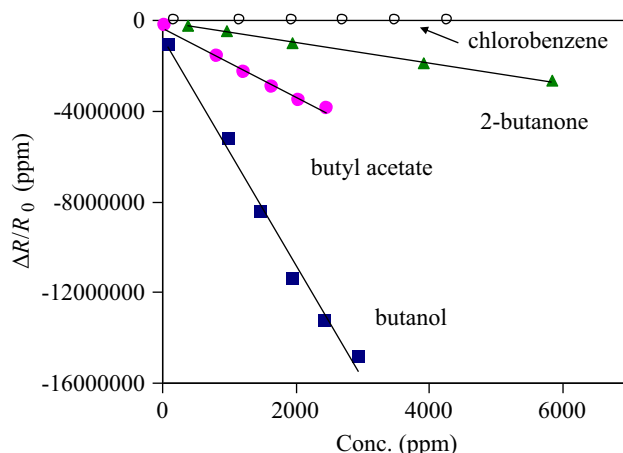


Fig. 8. Calibration curves of four polar compounds tested with a SWCNT-COOH coated chemiresistor.

carboxylic acid groups on adjacent SWCNT-COOHs inhibited the swelling completely and resulted in the lack of a response to nonpolar compounds in chemiresistor (Fig. 6).

Fig. 8 shows the calibration curves of several polar organic vapors that were tested using a SWCNT-COOH chemiresistor. Similar to toluene or octane, chlorobenzene showed only a barely detectable response on a SWCNT-COOH chemiresistor. The remaining compounds in Fig. 8 were able to either accept or partially stabilize the positive charge (i.e., proton) from carboxylic terminals. The responses of these compounds were all “negative,” which equated to a reduction in film resistance. In addition, unlike the other three swelling-

dependent chemiresistors, the negative calibration curves of SWCNT-COOH were all linear, which indicated clear differences in the response mechanism. Salehi-Khojin et al. recently proved that modulation of the conductivity of carbon nanotubes itself plays an important role in highly defected SWCNTs [45]. In the present study, the reactions of covalent modifications (i.e., acidification) created a highly defective SWCNT. All these polar organics in Fig. 8 were basic related to carboxylic acid. With the mechanism that we proposed in Fig. 6, these molecules attracted protons via hydrogen bonds accepting and releasing some of the electron density back to the carbon nanotubes, thus, the conductivity of the chemiresistor was increased. We have

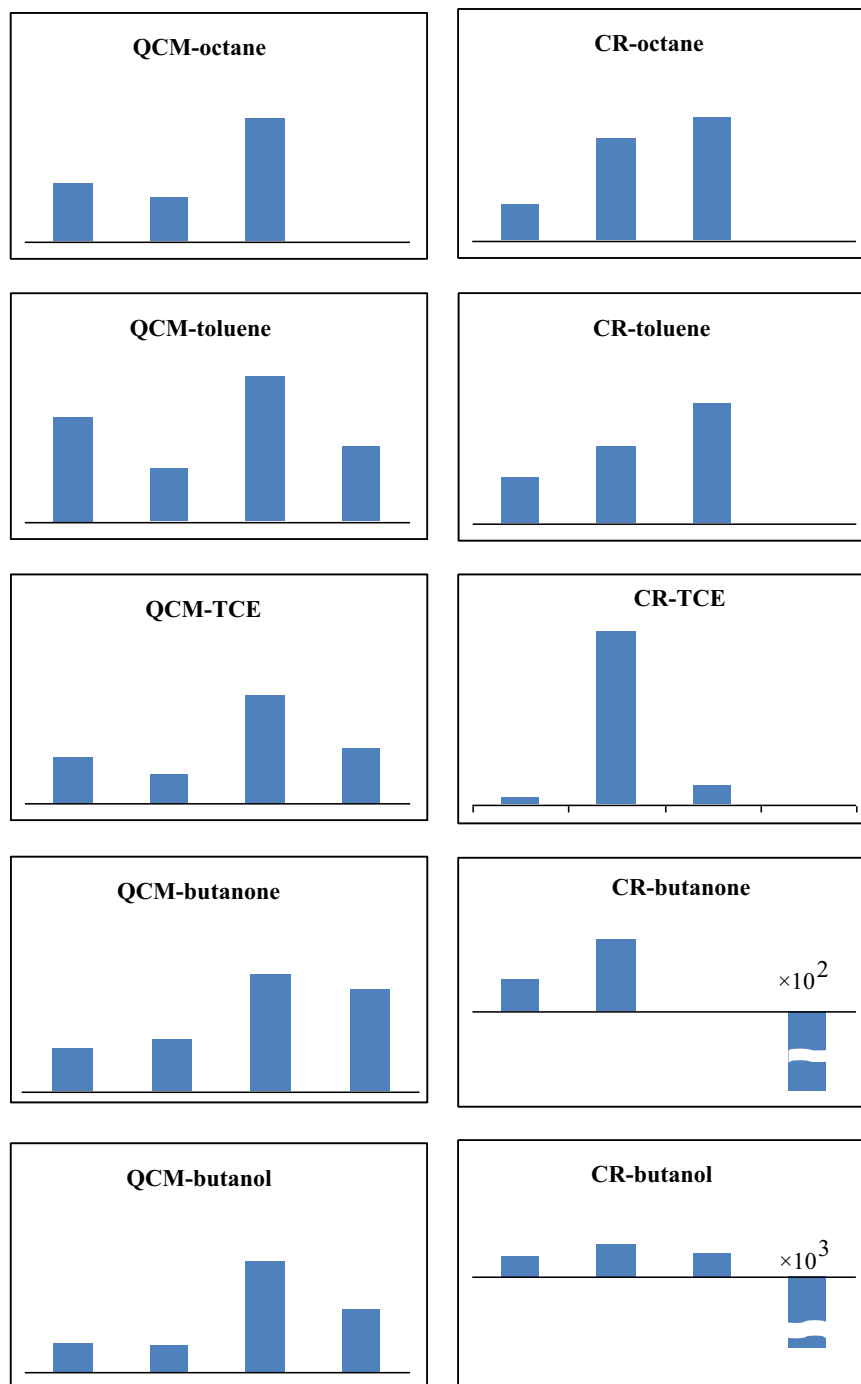


Fig. 9. Response patterns of five VOCs obtained from SWCNT-coated QCM and chemiresistor arrays. Coatings (from left to right): SWCNT, SWCNT-ESTER, SWCNT-SDS, SWCNT-COOH.

also tested several nonpolar organic vapors such as xylene and trichloroethylene, and none of these compounds showed measurable responses on the SWCNT-COOH chemiresistor.

3.5. QCM and chemiresistor response patterns

Response patterns are usually plotted as either a bar chart or a radar chart that shows the relative sensitivity of a sensor array to a target analyte. The most common approach is to normalize the sensitivity (i.e., calibration slope) with respect to the highest sensitivity in the sensor array. In the present study we plotted the response pattern of a QCM array in a conventional manner for five tested vapors, as shown in Fig. 9a–e. The extraction of response patterns from chemiresistor calibrations is somewhat difficult because the calibrations of swelling-dependent chemiresistors are nonlinear over the tested concentration range. We used the first portion of a calibration curve at low concentration range that could be approximated as a straight line, and then used the slope of this section to draw the response patterns (Fig. 9f–j).

The response patterns of the QCM arrays indicated that the surface modifications with SDS coating significantly increased the amount of absorption mass for most compounds. The covalent modification of a SWCNT into a COOH or ester group can alter the preferences to different functional groups to some degree. The response patterns of the chemiresistors were dramatically different from those of the QCM arrays. Despite the unique sensing behavior of the SWCNT-COOH chemiresistor, the relative sensitivities of the other three chemiresistors were also highly distinguishable. The additional mechanisms that were involved in the resistive changes led to the differences between chemiresistor and QCM patterns. It is noteworthy that the same set of SWCNTs can express different response patterns on two different sensor platforms. The versatile properties of sensing materials and the choice of proper sensing platforms are essential for constructing a hybrid array [46]. This discrepancy between QCMs and chemiresistors can be used to create a hybrid array that can potentially improve the recognition rate for vapors.

In the present study, the covalent surface modification started with converting a pristine SWCNT to a SWCNT-COOH. Dramatic changes in chemiresistor selectivity were observed: insensitive to nonpolar compounds and an increase in conductivity versus polar compounds. When the carboxyl acid groups further reacted to esters, these characteristics disappeared and the behavior of SWCNT-ESTER chemiresistors returned to swelling-dependent. This result indicated that the proton of a carboxyl acid plays an essential role in the unique response selectivity of a SWCNT-COOH chemiresistor.

4. Conclusion

In the present study, QCM and chemiresistor platforms were used to investigate the selectivity mechanisms of one pristine and three surface-modified SWCNTs. The results of the QCM provided a direct indication of the VOC partition selectivity of SWCNT surfaces. The chemiresistors responded to either swelling or charge modulation depending on the type of SWCNT. Surface-acidified SWCNT-COOHs showed a unique H-bond interlock that prohibited the swelling mechanism. However, the resistance of SWCNT-COOHs could be modulated via H-bond formation. The response time, linearity and relative sensitivities were all different between QCM and chemiresistor arrays coated with the same set of SWCNTs. The signal transduction mechanisms behind SWCNT-coated QCMs and chemiresistors were quite different, which implies that the diversified properties of surface-modified SWCNTs can be used to create a highly selective hybrid array.

Acknowledgements

The funding for this work was supported by the National Science Council of Taiwan under the project number NSC-100-2113-M-003-001-MY2.

Appendix A. Supporting information

Supplementary data associated with this article can be found in the online version at <http://dx.doi.org/10.1016/j.talanta.2014.08.027>.

References

- [1] L. Mølhave, *Indoor Air* 1 (1991) 357–376.
- [2] B. Tolnai, J. Hlavay, D. Möller, H.-J. Prümke, H. Becker, M. Dostler, *Microchem. J.* 67 (2000) 163–169.
- [3] J. Gutiérrez, M.C. Horrillo, *Talanta* 124 (2014) 95–105.
- [4] D.L. García-González, N. Tena, R. Aparicio-Ruiz, R. Aparicio, *Talanta* 120 (2014) 342–348.
- [5] C.L. Li, C.J. Lu, *Talanta* 79 (2009) 851–855.
- [6] S.J. Patrash, E.T. Zellers, *Anal. Chem.* 65 (1993) 2055–2066.
- [7] J.C. Echeverría, P. Vicente, J. Estella, J.J. Garrido, *Talanta* 99 (2012) 433–440.
- [8] Y.Q. Chen, C.J. Lu, *Sens. Actuators, B* 135 (2009) 492–498.
- [9] K.J. Chen, C.J. Lu, *Talanta* 73 (2007) 358–365.
- [10] W.H. Steinecker, M.P. Rowe, E.T. Zellers, *Anal. Chem.* 79 (2007) 4977–4986.
- [11] C.Y. Yang, C.L. Li, C.J. Lu, *Anal. Chim. Acta* 565 (2006) 17–26.
- [12] R.S. Jian, R.X. Huang, C.J. Lu, *Talanta* 88 (2012) 160–167.
- [13] M.A. Andio, P.N. Browning, P.A. Morris, S.A. Akbar, *Sens. Actuators, B* 165 (2012) 13–18.
- [14] E.S. Snow, F.K. Perkins, J.A. Robinson, *Chem. Soc. Rev.* 35 (2006) 790–798.
- [15] S. Basu, P. Bhattacharyya, *Sens. Actuators, B* 173 (2012) 1–21.
- [16] T.T. Tung, M. Castro, T.Y. Kim, K.S. Suh, J.F. Feller, *J. Mater. Chem.* 2 (2012) 21754–21766.
- [17] I. Sayago, H. Santos, M.C. Horrillo, M. Aleixandre, M.J. Fernández, E. Terrado, I. Tacchini, R. Aroz, W.K. Maser, A.M. Benito, M.T. Martínez, J. Gutiérrez, E. Muñoz, *Talanta* 77 (2008) 758–764.
- [18] J. Kong, N.R. Franklin, C. Zhou, M.G. Chapline, S. Peng, K. Cho, H. Dai, *Science* 287 (2000) 622–625.
- [19] J. Li, Y. Lu, Q. Ye, M. Cinke, J. Han, M. Meyyappan, *Nano Lett.* 3 (2003) 929–933.
- [20] M. Consales, S. Campopiano, A. Cutolo, M. Penza, P. Aversa, G. Cassano, M. Giordano, A. Cusano, *Sens. Actuators, B* 118 (2006) 232–242.
- [21] L. Lvova, M. Mastroianni, G. Pomarico, M. Santonico, G. Pennazza, C. Di Natale, R. Paolesse, A. D'Amico, *Sens. Actuators, B* 170 (2012) 163–171.
- [22] C. Viespe, C. Grigoriu, *Sens. Actuators, B* 147 (2010) 43–47.
- [23] I. Sayago, M.J. Fernández, J.L. Fontecha, M.C. Horrillo, C. Vera, I. Obieta, I. Bustero, *Sens. Actuators, B* 156 (2011) 1–5.
- [24] S. Manivannan, A.M. Saranya, B. Renganathan, D. Sastikumar, G. Gobi, *Kyu Chang Park, Sens. Actuators, B* 171–172 (2012) 634–638.
- [25] D.R. Kauffman, A. Star, *Angew. Chem. Int. Ed.* 47 (2008) 6550–6570.
- [26] U. Tisch, H. Haick, *J. Breath Res* 8 (2014) 1–8.
- [27] C. Di Natale, R. Paolesse, E. Martinelli, R. Capuano, *Anal. Chim. Acta* 824 (2014) 1–17.
- [28] S. Liu, Q. Shen, Y. Cao, L. Gan, Z. Wang, M.L. Steigerwald, X. Guo, *Coord. Chem. Rev.* 254 (2010) 1101–1116.
- [29] J. Lu, J.F. Feller, B. Kumar, M. Castro, Y.S. Kim, Y.T. Park, J.C. Grunlan, *Sens. Actuators, B* 155 (2011) 28–36.
- [30] S. Badhulika, N.V. Myung, A. Mulchandani, *Talanta* 123 (2014) 109–114.
- [31] B. Kumar, M. Castro, J.F. Feller, *Sens. Actuators, B* 161 (2012) 621–628.
- [32] Y.L. Zhao, J.F. Stoddart, *Acc. Chem. Res.* 42 (2008) 1161–1171.
- [33] B. Kumar, M. Castro, J.F. Feller, *Chem. Senses* 3 (2013) 1–7.
- [34] K. Balasubramanian, M. Burghard, *Small* 1 (2005) 180–192.
- [35] F. Wang, T.M. Swager, *J. Am. Chem. Soc.* 133 (2011) 11181–11193.
- [36] M. Penza, R. Rossi, M. Alvisi, M.A. Signore, E. Serra, R. Paolesse, A. D'Amico, C. Di Natale, *Sens. Actuators, B* 144 (2010) 387–394.
- [37] M.D. Shirsat, T. Sarkar, J. Kakoullis Jr., N.V. Myung, B. Konnanath, A. Spanias, A. Mulchandani, *J. Phys. Chem. C* 116 (2012) 3845–3850.
- [38] B. Esser, J.M. Schnorr, T.M. Swager, *Angew. Chem. Int. Ed.* 51 (2012) 5752–5756.
- [39] A. Star, T.-R. Han, V. Joshi, J.P. Gabriel, G. Gruner, *Adv. Mater.* 16 (2004) 2049–2052.
- [40] A. Star, J.P. Gabriel, K. Brasley, G. Gruner, *Nano Lett.* 3 (2003) 459–463.
- [41] N. Peng, Q. Zhang, C.L. Chow, O.K. Tan, N. Marzari, *Nano Lett.* 9 (2009) 1626–1630.
- [42] J. Lu, B. Kumar, M. Castro, J.F. Feller, *Sens. Actuators, B* 140 (2009) 451–460.
- [43] A. Bouvree, J.F. Feller, M. Castro, Y. Grohens, M. Rinaudo, *Sens. Actuators, B* 138 (2009) 138–147.
- [44] B. Kumar, J.F. Feller, M. Castro, *J. Lu, Talanta* 81 (2010) 908–915.
- [45] A. Salehi-Khojin, F. Khalili-Araghi, M.A. Kuroda, K.Y. Lin, J.-P. Leburton, R. I. Masel, *ACS Nano* 5 (2011) 153–158.
- [46] C.L. Li, Y.F. Chen, M.H. Liu, C.J. Lu, *Sens. Actuators, B* 169 (2012) 349–359.